Journal of Chemical and Petroleum Engineering (JChPE)

Print ISSN: 2423-673X Online ISSN: 2423-6721

Modeling and Optimization of Thermal Conductivity of Stabilized γ-Al_2O_3/Water Nanofluid Using Response Surface Methodology (RSM)

Behrouz Raei*

1. Department of Chemical Engineering, Mahshahr Branch, Islamic Azad University, Mahshahr, Iran. E-mail: behrouz.raei@iau.ac.ir

ARTICLE INFO

Article History:
Received: 03 July 2024
Revised: 02 October 2024
Accepted: 15 September 2024
Published: 02 October 2024

Article type: Research

Keywords:
DLS,
Optimum,
Sedimentation,
Stability,
Standard Deviation

ABSTRACT

The present study estimates the thermal conductivity ratio (KR) of stabilized γ-Al_2O_3/water nanofluid by response surface methodology (RSM). This study was conducted under experimental conditions with solid volume fractions of SVF = 0.05–2% and T = 25–45 °C temperature. Sedimentation visualization and dynamic light scattering (DLS) were performed to test the stability of nanofluids. The results of monitoring the stability of the nanofluid with the sedimentation visualization method showed that it was stable for at least 24 hours. Different models were evaluated based on a series of quality indicators and charts. Some indicators that were investigated in this study include standard deviation (Std. Dev.), coefficient of determination (R^2), and coefficient of variation (C.V.). After checking the quality indicators and charts for different models, the quadratic model was selected as the optimal model—the values of Std. Dev, R^2, and C.V. for the quadratic model were 0.0241, 0.9785, and 1.87, respectively. Also, adjusted R^2 and predicted R^2 parameters of the quadratic model were equal to 0.9606 and 0.8776, respectively, which signifies the model's accuracy. The residual plot, the standard probability plot, the Box-Cox plot, and the predicted vs. actual plot also showed that the quadratic model has good accuracy and is capable of estimating the KR of the nanofluid. The most optimum KR is 1.485. At a temperature of 45 °C, this condition was achieved in samples at SVF = 1.764%.

Introduction

In many engineering applications, base fluids like water, oils, and glycols are utilized as operational fluids in heat exchange systems. Improving the base fluids' thermal conductivity can raise the devices' thermal efficiency. The idea that solid particles the size of nanometers can disperse in base fluids was evolved by Choi et al. [1] and has grown to be a significant subject known as nanofluids. In order to be able to research nanofluids, preparing these types of fluids in a stable form is a very important factor because the stability of nanofluids strongly affects their thermophysical properties [2, 3]. The type, size, shape, concentration, base fluid, operating temperature, and addition of surfactant all affect the thermophysical properties of dispersed nanoparticles in nanofluids [4-6]. In addition, although augmenting the nanoparticle concentration enriches the thermophysical features of the nanofluid, there is a penalty for changing the stability behavior [7-9]. Hence, optimizing parameters poses a significant challenge for researchers [10].Thermal conductivity is a crucial physical feature of nanofluids

* Corresponding Author: B. Raei (E-mail address: behrouz.raei@iau.ac.ir)

Publisher: University of Tehran Press *DOI: 10.22059/jchpe.2024.378620.1531*

that warrants further investigation. As a result, numerous researchers have accomplished various experimental and numerical studies to determine the thermophysical features of nanofluids [11-20]. It is crucial to research the factors that have an important effect on these features. Numerous researchers have looked into the thermophysical features of varied nanoparticles in current years in various base fluids [21-28]. Esfe et al. [29] accomplished a laboratory examination of the thermal conductivity of nanofluids suspended in water, including five nm-diameter Al_2O_3 nanoparticles. The thermal conductivity of Al_2O_3/water was measured within a temperature range of 26 to 55 °C. The findings demonstrated that raising the temperature at any concentration significantly increased the thermal conductivity of nanofluids. Putra et al. [30] experimentally studied the thermal conductivity of Al_2O_3/water nanofluid with an average nanoparticle size of 131 nm. The findings proved that the nanofluid's thermal conductivity rose by approximately 24% when the concentration was increased to 4%. Zhang et al. [31] have performed an experimental study to find how Al_2O_3/water nanofluid concentration affected the thermal conductivity. The thermal conductivity increased by 15% when the concentration was increased to 5%. Masuda et al. [32] researched the thermal conductivity of titanium oxide and aluminum oxide in water-based fluid through experimentation. They demonstrated that these nanofluids' thermal conductivity increases by 10% and 30%, respectively when compared to water at a concentration of 4%. Eastman et al. [33] observed a 40% rise in CuO-EG nanofluid thermal conductivity at 0.3 vol%. Murshed et al. [34] investigated the thermal conductivity of water-based titanium oxide nanofluid with rod and spherical forms. Their findings demonstrated that the shape of the particles is a significant factor in raising the thermal conductivity of the nanofluid. After comparing the experimental outcomes with theoretical models, it was discovered that the thermal conductivity values of nanofluids obtained from experiments were higher than those estimated by the models. Mintsa et al. [35] have documented that concentration and temperature enhance thermal conductivity in nanofluids of copper oxide (47 nm) and aluminum oxide (36 nm). A study by Abdel-Samad et al. [36] has demonstrated that as temperature and concentration rise, the thermal conductivity of the titanium oxide-water nanofluid accelerates. They found that at 90°C, there was an increase in thermal conductivity of 37.35% with a volume fraction of 0.47%, whereas at 20 °C, there was an increase of 24.11%. Eshgarf et al. [37] investigated an iron oxide-water nanofluid's viscosity and thermal conductivity at various temperatures and concentrations. Next, artificial neural networks (ANNs) were utilized to progress models for forecasting the thermophysical properties mentioned. According to these findings, the suggested models could accurately forecast nanofluids' thermophysical characteristics. The statistical modeling method known as response surface methodology (RSM) describes the interconnectivity of system inputs and outputs using mathematical models [38]. The ability of RSM to capture the non-linear relationships between the inputs and the outputs has demonstrated its effectiveness in modeling the thermophysical characteristics of nanofluids [39, 40]. Peng et al. [41] have presented the findings of a trustworthy model utilizing RSM to predict the thermal conductivity of CuO/water nanofluid at varied temperatures and concentrations. Esfe et al. [42] examined the rheological behavior of the HNF (Hybrid Nanofluid) containing MWCNT-SiO_2 (10:90) with the RSM. The main objective of this study was to introduce a new correlation. Khetib et al. [43] used RSM to investigate the viscosity of a paraffin-based CuO nanofluid. Experiments conducted at T = 25–100 °C and mass fractions of 0 –25% provided the data used in the modeling. RSM shows that the results obtained from the third-degree polynomials are more accurate compared to second-degree and linear polynomials. Table 1 shows an overview of prior research on using RSM in estimating nanofluids' thermal conductivity.

Table 1. Applications RSM in forecasting thermal conductivity of nanofluid

References	Nanoparticles	Base fluid	Remarks
Peng et al.[41]	CuO (II)	Water	R^2 = 0.9939 AAD% = 0.615%
Esfe et al.[44]	Al_2O_3	EG/water	R^2 = 0.9982,
Esfe & Hajmohammad [22]	ND + Co_3O_4	EG/water	R^2 = 0.9957 Std. Dev = 0.002516
Khetib et al. [45]	ND + Fe_3O_4	EG/water	R^2 = 0.994 MSE = 2.0297×10-6
Khetib et al.[46]	Fe_3O_4	Water	R^2 = 0.998 MSE = 0.0013
Malika & Sonawane [39]	Fe_3O_4+ SiC	Water	R^2 = 0.969 AAD% = 1.165%
Shahsavar et al.[47]	GO + Fe_2O_3 + TiO_2	Oil	R^2 = 0.9898 Adjusted R^2 = 0.9895 Predicted R^2 = 0.9888 Std. Dev = 0.1856 C.V% = 1.31%
Borode & Olubambi [48]	GNP + Al_2O_3	Water	R^2 = 0.9882 Adjusted R^2 = 0.9840 Predicted R^2 = 0.9721 Std. Dev = 0.0020 C.V% = 0.3263%
Esfe et al.[49]	MWCNT + Al_2O_3 + ZnO	Water	R^2 = 0.9972 Adjusted R^2 = 0.9968 Predicted R^2 = 0.9962 Std. Dev = 4.447 ×10-3 C.V% = 0.4% -1.05% < MOD < + 1.08%
Esfe et al.[50]	MWCNT + TiO_2	EG/water	R^2 = 0.9957 Adjusted R^2 = 0.9934 Predicted R^2 = 0.9909 Std. Dev = 0.0082 C.V% = 0.6799% -1.754% < CD% < + 0.9615%

AAD: average absolute deviation
C.D: correlation deviation
C.V: coefficient of variation
Std. Dev: standard deviation
R2: coefficient of determination
MOD: margin of deviation
MSE: mean square error
GNP: graphene nanoplatelets
ND: Nanodiamond

The first part of this study deals with preparing Al_2O_3/water nanofluid, stabilization method, and stability measurements. Then, the process of measuring thermal conductivity is defined. The reasons for choosing Al_2O_3 nanoparticles are its desirable features such as reasonable price, the possibility of various applications, availability with high purity, high thermal and corrosion resistance, strength and high degree of mechanical hardness, and favorable environmental compatibility. Then, the design of the experiment, the model's formation, and the model's accuracy with respect to the experimental data are investigated using Design Expert software (13.0.0).

We establish a correlation dependent on the interaction of operating parameters and evaluate its reliability with experimental data. Based on the literature, it can be realized that most of the models developed for the prediction of thermal conductivity have certain limitations that limit the application of the correlations to other nanofluids. So, the primary objective of this work is to evaluate the possible effect of the operating temperature and also the SVF (solid volume fraction) and their interactions on the thermal conductivity of the nanofluid. The other goal of this study is the optimization of parameters to maximize the thermal conductivity of the system using RSM. The last goal of this research was to compare the outcomes of the estimation of the RSM model with other models presented in the literature.

Nanofluid Preparation and Property Measurement

Nanofluid Preparation and Stability Check

There are two methods for nanofluid production, including one-step and two-step. Due to the commercial availability of nanoparticles, numerous researchers have developed a two-part process for manufacturing nanofluid. Specification of γ-alumina nanoparticles (obtained from US Research Nanomaterials, Inc.) is displayed in Table 2. Transmission electron microscopy (TEM) was employed to estimate the size of primary nanoparticles. Based on the illustration in Fig. 1, it is evident that the nanoparticles have an approximately spherical shape.

Table 2. Specification of nanoparticle used in this study

Nanoparticle	Aluminum Oxide (gamma)
Average particle size (nm)	20
Purity	>99%
Density (kg/m^3)	3890
Color	White
Morphology	Nearly spherical
Specific area (m^2/g)	>138
Specific heat (J /kg K)	880
Thermal conductivity (W/m K)	46

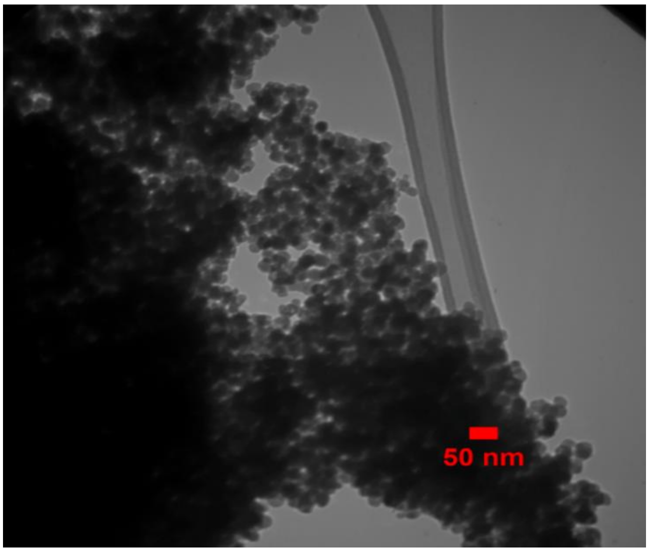

Fig. 1. Image of TEM nanoparticles used in this study

In this study, a two-step method was used to prepare nanofluids. The stability of nanofluids is a significant concern in this technique. Thermophysical and heat transfer properties are closely tied to the stability of a nanofluid [51]. The long-term stability of nanofluids is a crucial factor in determining their practical applicability. In this study, the nanofluids' concentration (0.05, 0.5, 1, and 2 vol%) and temperature (25, 35, and 45 °C) were chosen. Alumina nanoparticles are added to distilled water as the base fluid, and their weight is measured in four decimal places. The fluid was stirred with a magnetic stirrer for one hour and then transferred to an ultrasonic vibrator (BANDELIN Company - power 240 W and frequency 35 kHz) for three hours. In this study, we employed sedimentation visualization and dynamic light scattering (DLS) to assess the stability of nanofluids. The results of monitoring the stability of nanofluid with the sedimentation visualization method showed that it was stable for at least 24 hours. The mentioned method is used in references [52-56]. DLS detects the size distribution of nanoparticles in the dispersed phase. DLS technique was employed to obtain particle size distribution in nanofluids using a Malvern Zetesizer Nano (Malvern Panalytical, UK) to study clustering and agglomeration phenomena. Fresh and old samples (after 7 days) were analyzed to determine the particle size distribution. The findings are outlined in Table 3. Because DLS measures the hydrodynamic radius of nanoparticles, the average size obtained by these particles was larger than what could be seen through a micrograph of TEM. The findings also indicate that a rise in the vol. fraction of nanofluid leads to a larger particle size. The increased agglomeration of nanoparticles upon their addition to the base fluid can be attributed to this phenomenon. In addition, the results show that freshly prepared nanofluids in different concentrations have larger average diameters of nanoparticles than nanofluids after 7 days old. Such a phenomenon is related to the fact that the larger aggregated particles settle, and this causes the easy detection of smaller particles by DLS [57, 58]. The mentioned findings agree with the results of studies [57, 59, 60].

Table 3. The average diameter of nanoparticles at different times obtained from dynamic light scattering (DLS)

Concentration (vol.%)	**Nanoparticle diameter (nm)**	
	freshly	7 days old
0.05	134	90
0.5	161	129
1	169	147
2	218	197

Measurement of Thermal Conductivity

A KD2 Pro thermal properties analyzer (Decagon Devices, Inc. USA, Fig. 2) was applied to measure the thermal conductivity of the nanofluid under different experimental conditions. The measurement works in the range of 0.02-2 W/m.K. This device is fitted with a KS-1 needle sensor placed vertically and centrally in the nanofluid container. The temperature of the sample was controlled with the aid of a water bath during the measurement process. To avoid the possibility of transient heat effects, a 30-minute interval between subsequent measurements was chosen to minimize their impact on the temperature increase near the probe. Therefore, the obtained results are stable and repeatable. To achieve precision and consistent results, the average of three thermal conductivity measurements for each sample is used. The uncertainties in thermal conductivity measurements were predicted based on the accuracies of the tools given in Table 4 and calculated by the method [61]. The maximum uncertainty in the measured thermal conductivity was 1.8 %.

Fig. 2. Thermal properties analyzer device

Table 4. Accuracy of the instruments

Instruments	Accuracy
Weighing balance	±0.0001
Ultrasonic bath	3 kHz±
Thermal conductivity apparatus	±0.01 W/m.K
Water bath	±0.1 °C

RSM

Many engineering phenomena have been modeled using theories. A suitable mathematical model for many phenomena is unavailable due to various controlling factors, computational complexity, or unknown mechanisms. Experimental modeling techniques are efficient. One of the approaches to experimental modeling is RSM. In this approach, the response variable is affected by numerous independent input parameters, aiming to optimize the response variable and analyze the factors impacting it while minimizing the number of tests conducted. Response surface methodology (RSM) has many applications in different topics such as essential oil [62] and seed oil extraction [63, 64], optimization and mathematical modeling [65, 66], impregnation [67, 68], nanoparticle formation [69-71], etc.

Results and Discussion

The RSM evaluation uses a statistical regression approach to model the correlation between the input variable SVF and T and the nanofluid output response variable (KR = thermal conductivity ratio = $\frac{K_{nf}}{K_{bf}}$). Table 5 displays the p-values, Adjusted R^2, and Predicted R^2 values for the linear, two-factor interaction (2FI), quadratic and cubic models that were examined in the analysis.

Table 5. Summary of statistics for the various models

Source	Sequential p-value	Adjusted R^2	Predicted R^2	
Linear	0.0002	0.8156	0.7353	
2FI	0.7769	0.7948	0.6797	
Quadratic	0.0030	0.9606	0.8776	Suggested
Cubic	0.2971	0.9534	0.8113	Aliased

The sequential p-value column denotes the importance level of each model term as they were sequentially added to the model. It quantifies the probability of achieving the recorded data or even more extreme results assuming the null hypothesis holds true. A p-value below 0.05 indicates that the term is statistically essential, signifying its impact on the variability of the response variable [72]. The Adjusted R^2 value indicates the proportion of the overall variance in the dependent variable determined by the model while also considering the number of independent variables included. A higher Adjusted R^2 value implies a better fit between the model and the data. The Predicted R^2 column displays the anticipated proportion of variability in forthcoming observations that the model can clarify. A greater Predicted R^2 value suggests that the model is expected to perform strongly when applied to new data. This table shows that the quadratic model has the best Adjusted R^2 (0.9606) and Predicted R^2 (0.8776), which is the most accurate model to provide the best fit to the data and estimate the response variable. The adjusted R^2 value for the cubic model is also high (0.9534), whereas the R^2 values for the 2FI and Linear models are comparatively lower. The Cubic model exhibits a low Predicted R^2 (0.8113) and is marked as Aliased, indicating that it cannot be differentiated from another model due to collinearity or confounding factors. Hence, this study has chosen the quadratic model for further examination. Table 6 displays the results of the ANOVA analysis for the quadratic model. The sources of variability are presented, along with their corresponding sum of squares, degrees of freedom, mean square, F-value, and p-value. The F-value is utilized in ANOVA to assess the statistical importance of the variation among factors [73]. The model is considered statistically significant with an F-value of 54.59, indicating that the probability of obtaining such a high F-value by random chance is extremely low at 0.01%. The results suggest that both factors, the SVF (A) and temperature (B), have extremely low p-values (<0.0003), signifying their significant influence on the response. Both the AB interaction term and B^2 have p-values that exceed 0.05, suggesting that they are not statistically significant. Conversely, A^2 possesses a p-value of 0.0012, denoting its significance as a term.

Table 6. ANOVA outcome for the suggested quadratic model

Source	Sum of Squares	Df	Mean Square	F-value	p-value	
Model	0.1581	5	0.0316	54.59	< 0.0001	significant
A-SVF	0.1134	1	0.1134	195.68	< 0.0001	
B-T	0.0337	1	0.0337	58.19	0.0003	
AB	0.0003	1	0.0003	0.4471	0.5286	
A^2	0.0193	1	0.0193	33.30	0.0012	
B^2	0.0014	1	0.0014	2.33	0.1778	
Residual	0.0035	6	0.0006			
Cor Total	0.1616	11				

Table 7 shows the fit statistics of the quadratic model. The table denotes that the Predicted R^2 value of 0.8776 nearly matches the Adjusted R^2 value of 0.9606, with a difference of less than 0.2. This indicates that the model can be trusted when making estimations for future observations. The Adeq Precision assesses the model's quality by comparing the variation in the data with the variation anticipated by the model. A ratio exceeding four is deemed satisfactory, and a viewed ratio of 23.2535 suggests that the model is suitable for exploring the design space.

Table 7. Fit statistics for the quadratic model

Std. Dev.	Mean	CV %	R^2	Adjusted R^2	Predicted R^2	Adeq Precision
0.0241	1.29	1.87	0.9785	0.9606	0.8776	23.2535

Table 8 exhibits the coefficient estimates, degrees of freedom, standard error, 95% confidence interval, and variance inflation factors (VIFs) for each factor in the *KR*. The coefficient estimate signifies the anticipated alteration in the response when the value of a factor changes by one unit while all other factors remain constant. In an orthogonal design, the intercept represents the mean response of all the runs. The coefficients indicate adjustments to the mean reaction according to the factor configurations. When the factors are orthogonal, the variance inflation factors (VIFs) will equal 1. VIFs exceeding 1 indicate the existence of multicollinearity, with a stronger correlation between factors as the VIF value increases. Typically, VIFs that are below 10 are considered acceptable. The intercept coefficient estimate is 1.34, which suggests the average response of all runs when all variables are set to their baseline values. The coefficient estimate for factor A (SVF) is 0.1318, indicating that a one-unit increase in SVF leads to a 0.1318 increase in the response, while all other factors remain constant. The factor B (temperature) has a coefficient estimate of 0.0661, suggesting that a one-unit increase in temperature leads to a response increase of 0.0661 while holding all other factors constant. The AB coefficient estimate is 0.0077, denoting that the interaction between factors A and B has a minor positive effect on the response. The coefficient estimate for A2 is -0.0920, indicating that a one-unit increase in A^2 leads to a reduction of 0.0920 in the reaction, while all other factors are held constant. The coefficient estimate for B^2 is 0.0225. Additionally, VIFs offer insights into the collinearity present among factors. In this instance, they are all near or below 1.04, indicating that collinearity is not a significant concern in the model.

Table 8. Coefficient estimate in terms of the coded factors

Factor	Coefficient Estimate	Df	Standard Error	95% CI Low	95% CI High	VIF
Intercept	1.34	1	0.0153	1.31	1.38	
A-SVF	0.1318	1	0.0094	0.1088	0.1549	1.02
B-T	0.0661	1	0.0087	0.0449	0.0873	1.04
AB	0.0077	1	0.0114	-0.0204	0.0357	1.04
A^2	-0.0920	1	0.0159	-0.1310	-0.0530	1.02
B^2	0.0225	1	0.0147	-0.0136	0.0586	1.0000

The relationship between the KR and the actual values of the SVF and T factors is illustrated in Eq. 1. The coefficients assigned to each factor determine their impact on KR. At the same time, the interaction term signifies the combined effect of both factors. This equation, different from the coded one, forecasts the actual response values in their original units. Nevertheless, it is impossible to compare the coefficients to assess each factor's relative strength, as they have been adjusted to match the units of each factor. Furthermore, the intercept does not depict the center of the design space.

$$KR = 1.17601 + 0.306159 * SVF - 0.009947 * T + 0.000785 * \mathrm{SVF} * T - 0.096795 * SVF^2 + 0.000225 * T^2 \quad (1)$$

The perturbation plot in Fig. 3 demonstrates the effect of two factors on the KR response. The diagram visually depicts the relationship between the examined factors and the system's response. The diagram is created by perturbing a single factor at a time while keeping the other factors fixed and monitoring the resulting alterations in the response. This permits you to visualize the curvature of the response surface and identify interactions between factors. The slope of each line demonstrates the sensitivity of the reaction to that particular factor. In contrast, the curvature of the line signifies the existence of any interactions with the other factors. According to Fig. 3, it can be viewed that factor A exerts the most significant influence on the KR, whereas factor B demonstrates the least impact.

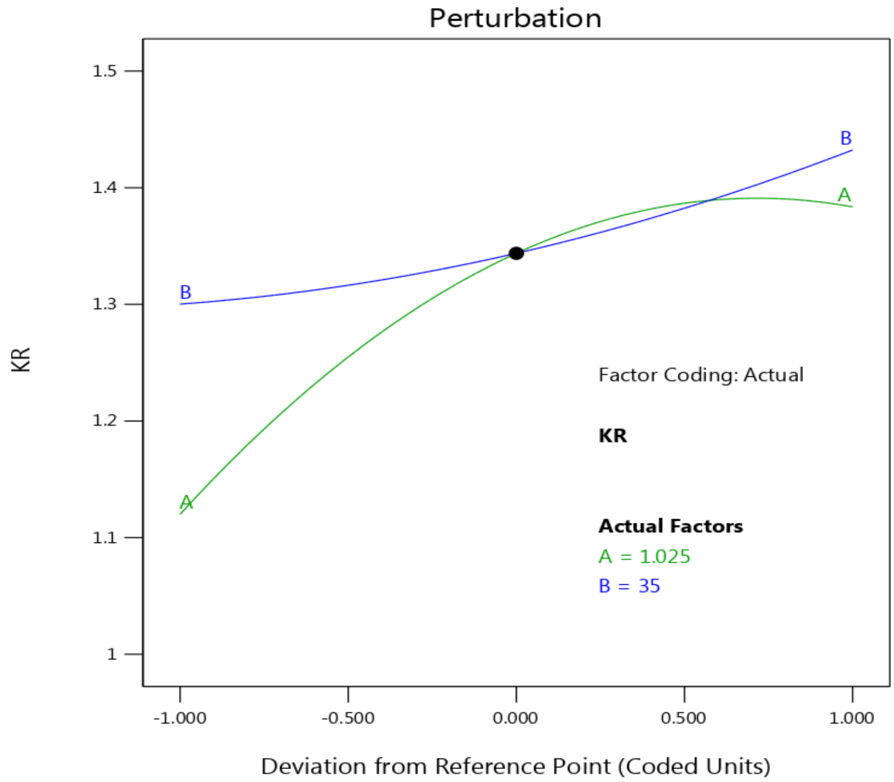

Fig. 3. Perturbation plot of the influence of input factors on the KR

Fig. 4 compares the outcomes gained from the experimental examination with the anticipated results deduced from the correlations suggested by RSM. Fig. 4 demonstrates that the actual and predicted outcomes are nearly similar, with just a few minor deviations, as evidenced by Fig. 5a-c. The studentized residual distribution is depicted in Fig. 5a, showing that most residuals are concentrated near the '0' reference line. This implies that the correlations established are reliable and the models accurately capture the behavior of the data. Furthermore, in Fig. 5b, one can observe a reasonably random distribution of residuals throughout the run order, suggesting that the model adequately addresses the temporal dimension of the data. Fig. 5c shows the normal probability graph of the selected model. This graph illustrates the normal distribution of the residuals and their linearity. Even for typical data, some degree of scattering can be expected. If the data follows an S-shaped curve, it is necessary to employ transfer functions. As shown in Fig. 5c, the selected model is linear primarily with minimal deviation. A standard probability plot is used to evaluate how a small data set is normally distributed.

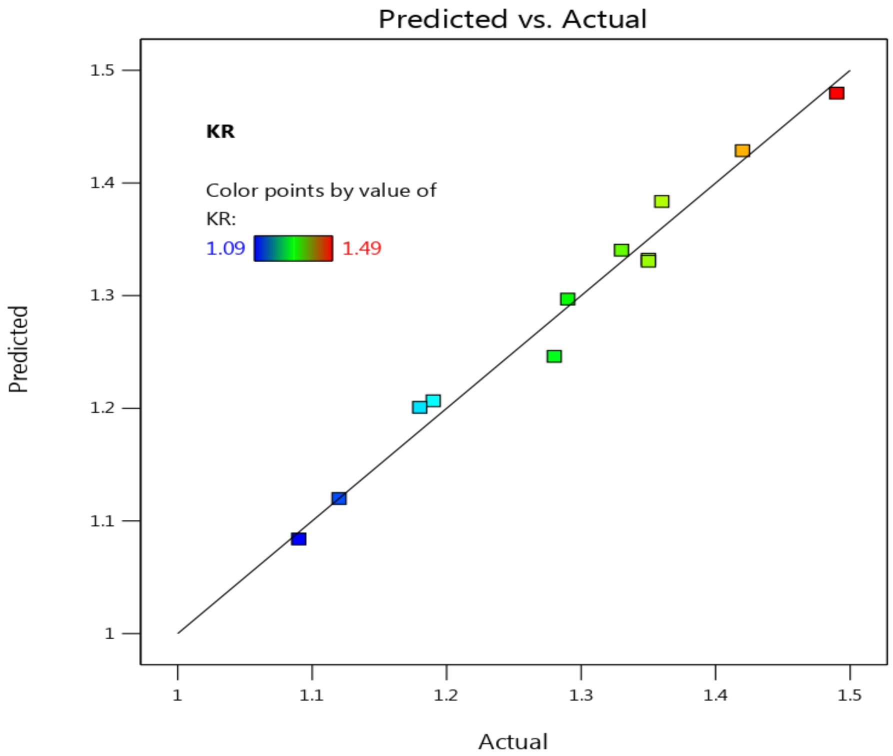

Fig. 4. Correlation between the experimental and predicted values

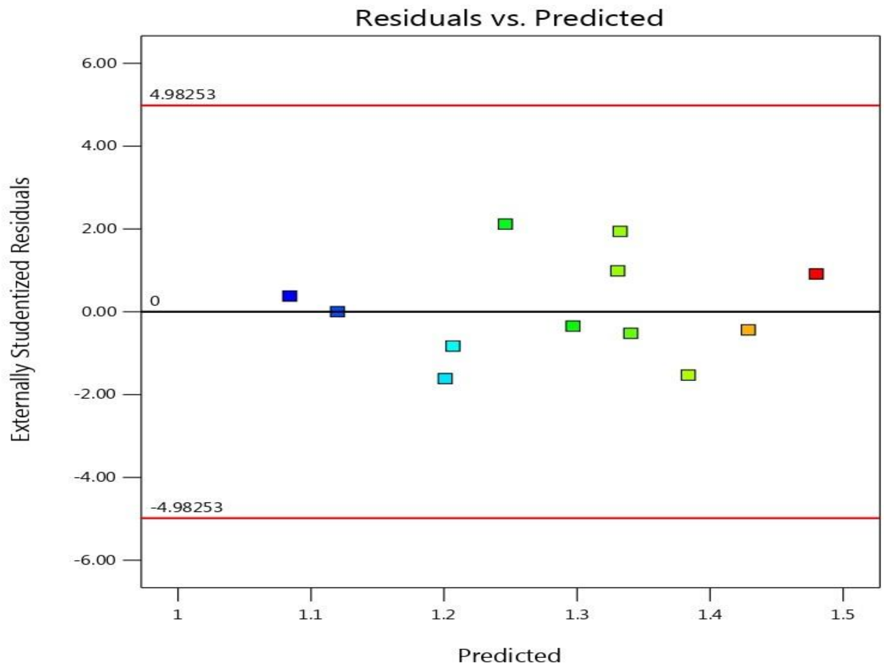

(a)

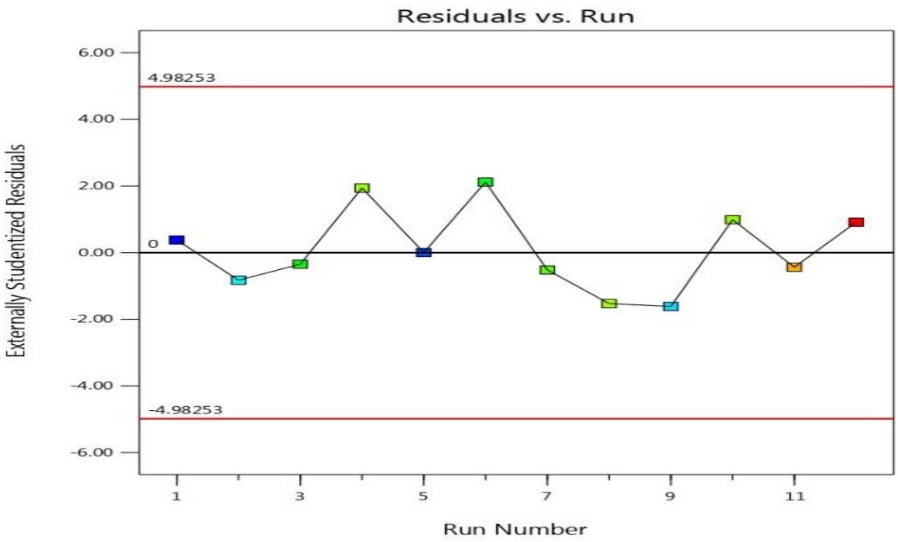

(b)

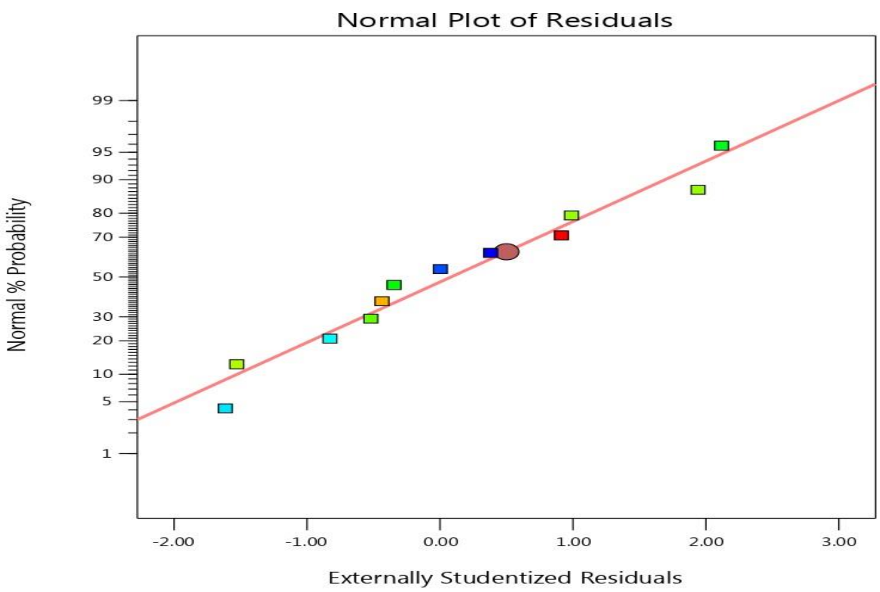

(c)

Fig. 5. Plot of externally studentized residuals in relation to (a) predicted value, (b) run order, (c) standard plot

A lambda value 1 in Box-Cox plot analysis indicates that the original data fits well. Box-Cox plots are utilized to transform the data distribution into a normal distribution. Fig. 6 displays the Box-Cox plots of the quadratic model. This plot offers guidance on selecting the appropriate transfer function. The optimal transfer function is recommended by considering the best lambda value situated at the curve's minimum point. The software will not suggest any transformation if the 95% confidence interval surrounding this lambda includes 1. As depicted in Fig. 6, the quadratic model plot exhibits suitable behavior, with the lambda line predominantly positioned at the lower bottom of the curve.

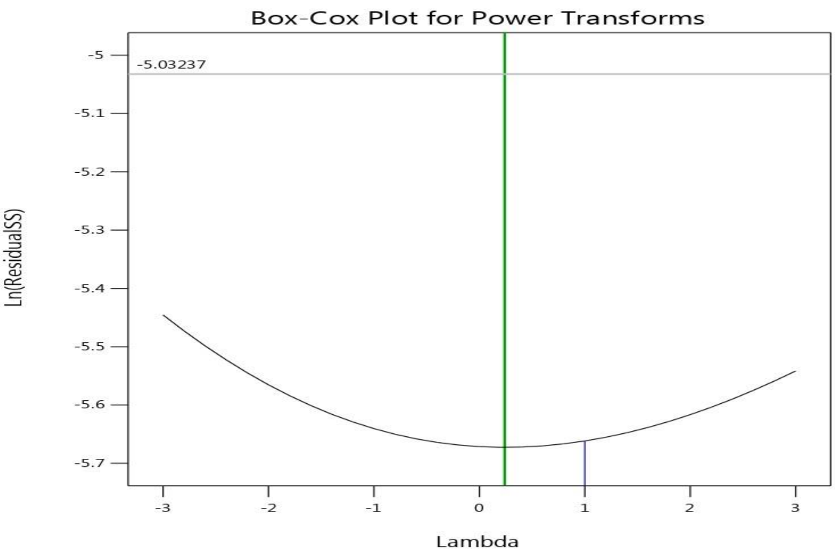

Fig. 6. Box-Cox diagrams for determining Lambda value. Current λ=1, Best λ=0.24, Recommended transform=none

The 2D contour and 3D surface plots in Figs. 7 & 8 demonstrate how different input parameters affect the KR of the nanofluid. Fig. 7 presents a 2D contour illustrating the effect of SVF and T on KR, which helps us understand their relationship. Instead, Fig. 8 improves deducing by exhibiting a three-dimensional surface plot that allows more detailed visualization of the complex interaction between SVF, T, and KR. The plot contour lines link points sharing the same KR value, enabling us to pinpoint regions with higher or lower KR values and detect trends or patterns. Figures indicate that the KR of the nanofluid enhances rapidly as the SVF level rises. Additionally, the statistics exhibit that the KR enhances as the temperature increases (although this effect is not tangible compared to the SVF.), which can be attributed to the rise in Brownian motion due to increasing temperatures. These results align with earlier research studies that have been published [74, 75].

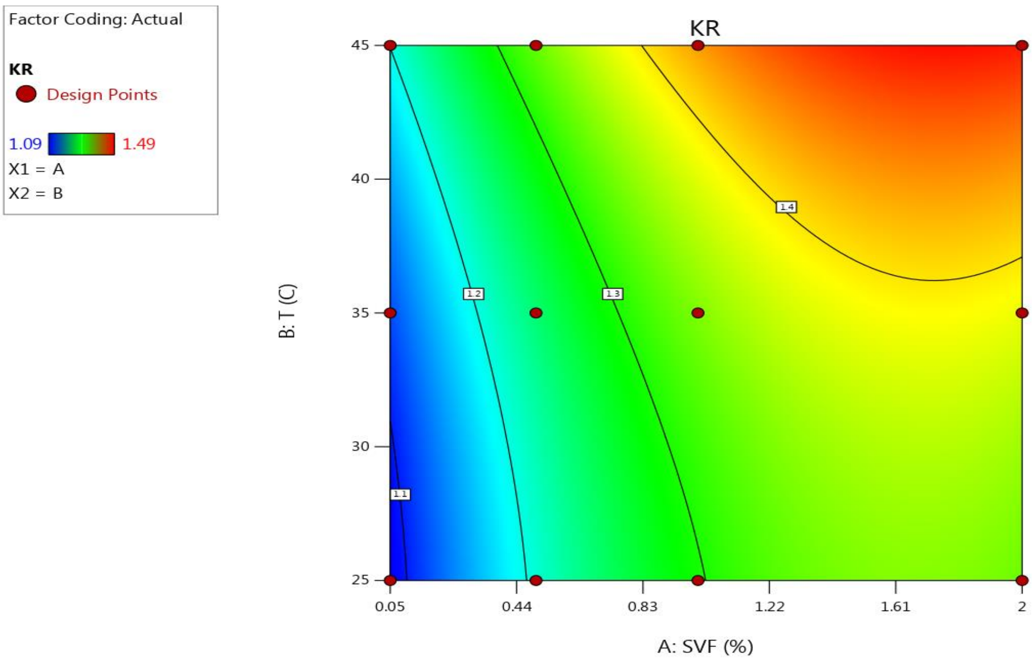

Fig. 7. 2D contour plot of the impact of SVF and T on the KR

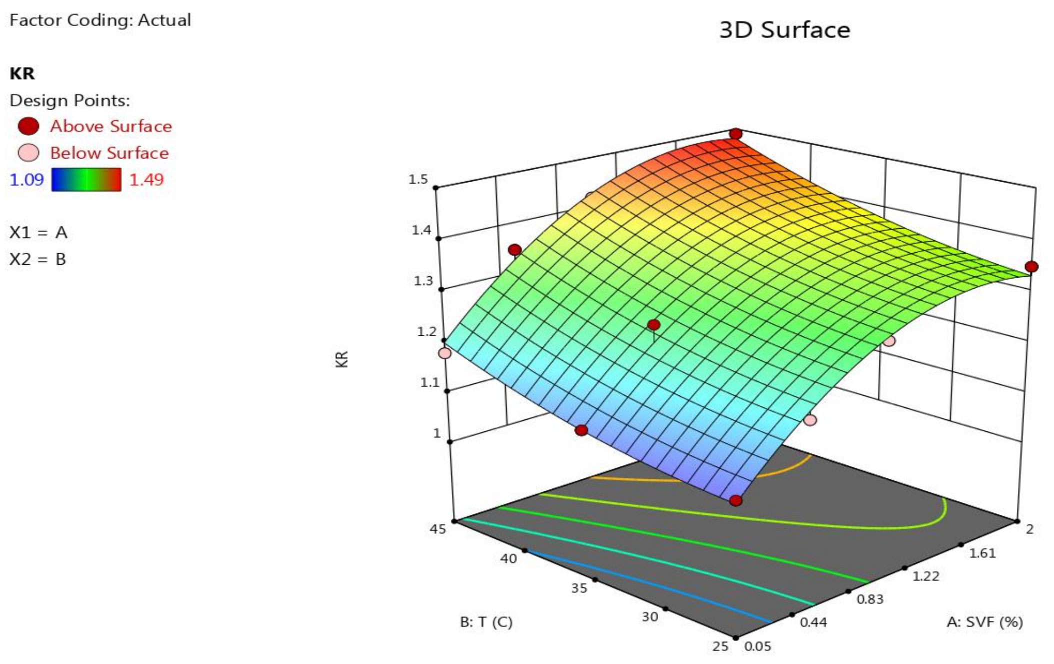

Fig. 8. 3D surface plot of the impact of SVF and T on the KR

Optimum Response

An optimization was performed on the thermal conductivity ratio (KR) of the Al_2O_3/water nanofluid to achieve its maximum value. This optimization involved adjusting the SVF and T of the nanofluid. In order to optimize the process, the KR of the nanofluid was maximized by utilizing the correlation acquired through RSM. The optimization results demonstrated that the nanofluid's KR is maximized at 45 ◦C, reaching 1.485, within the investigated range of T (25 to 45 ◦C) and SVF (0.05 to 2% vol.). Achieving this value is possible only when the SVF of the nanofluid is adjusted to 1.764%. Table 9 showcases a range of optimal solutions for nanofluid. Fig. 9a & b displays the desirability value and optimal KR values at different points.

Table 9. Different optimal solutions for nanofluid

Number	SVF	T	KR	Desirability	
1	1.764	45.000	1.485	0.988	Selected
2	1.754	45.000	1.485	0.988	
3	1.780	45.000	1.485	0.988	
4	1.744	45.000	1.485	0.988	
5	1.808	45.000	1.485	0.988	
6	1.879	45.000	1.484	0.985	
7	1.598	45.000	1.483	0.981	
8	1.578	45.000	1.482	0.980	
9	2.000	44.046	1.469	0.947	

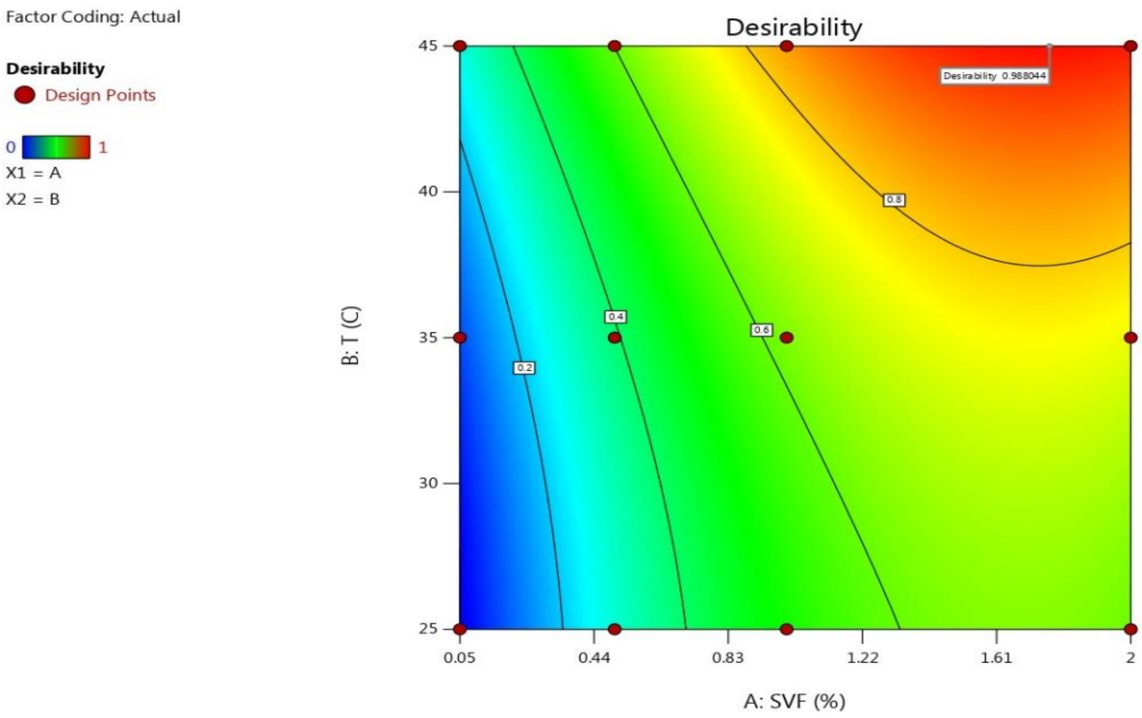

(a)

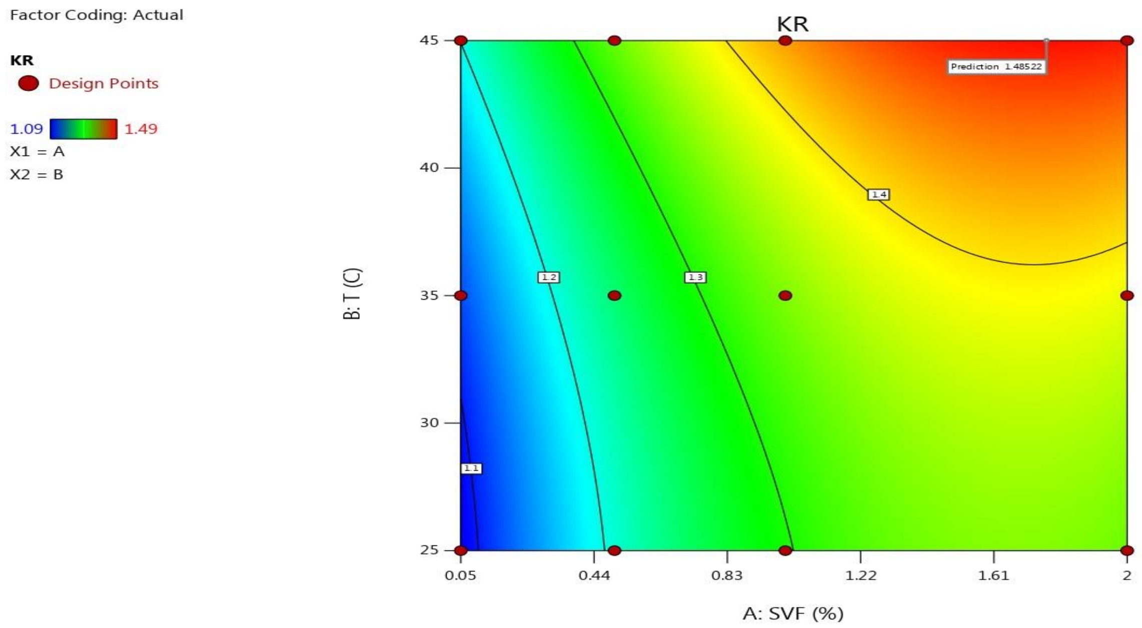

(b)

Fig. 9. Optimal values of KR in different SVF (a) desirability (b) KR

Fig. 10 compares the proposed RSM model with other theoretical and experimental models in the literature to estimate the KR of the nanofluid. As it is clear from Fig. 10, other models performed poorly in estimation, while the RSM model has a very good match with the experimental data. Also, in Table 10, the comparison of different models has been done quantitatively and with different statistical parameters. The table clearly shows that the best results are related to the RSM model for all statistical parameters. The mentioned findings are in agreement with the results [76]. Table 11 displays the mathematical representation of statistical parameters employed in this research.

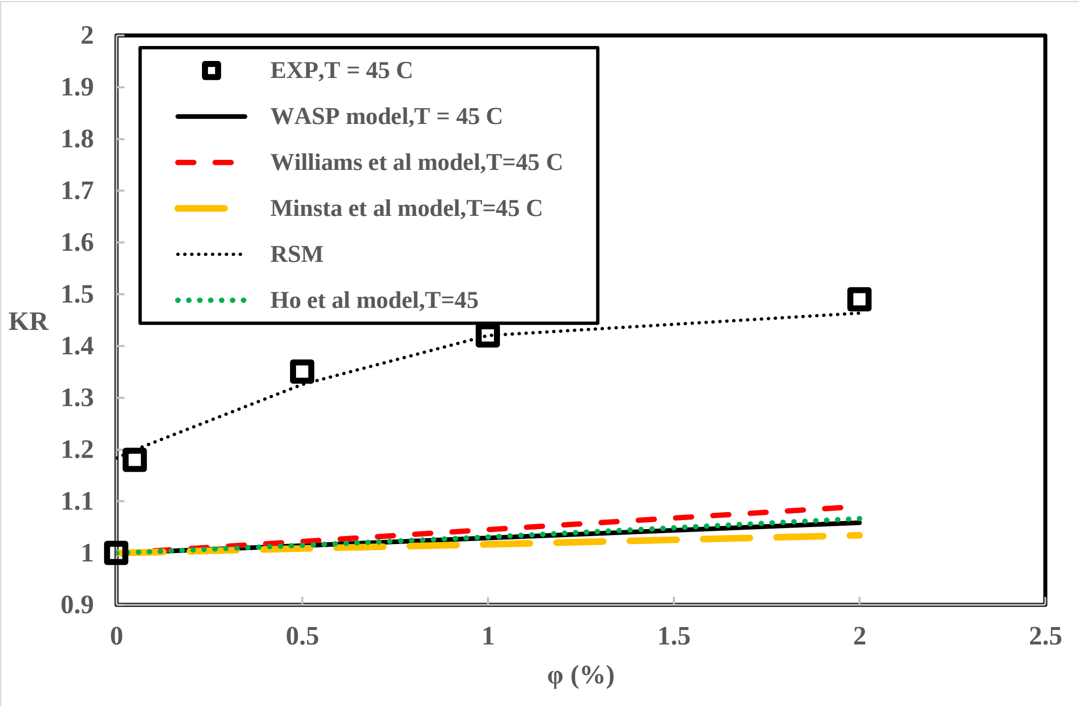

Fig.10. Comparison of different models in the forecasting of KR nanofluid

Table 10. The comparison between the results of the RSM model and other models for the estimation of KR nanofluid

Models	AARD%	MSE	RMSE	Maximum MOD%
WASP [77]	19.3	0.097	0.311	29.2
Williams et al. [78]	18.5	0.088	0.297	26.9
Mintsa et al. [35]	20.1	0.1	0.323	31.4
Ho et al. [79]	19.2	0.095	0.308	28.4
RSM	3.7	0.007	0.0841	14.3

Table 11. The mathematical expressions of statistical parameters used in this study

Statistical parameters	Formula
Average absolute relative deviation percent (AARD%) [80]	$AARD\% = \frac{100}{n}\sum_i \frac{\lvert P_{iexp} - P_{ipred}\rvert}{P_{iexp}}$
MSE [80]	$MSE = \frac{1}{n}\sum_i \left(\lvert P_{iexp} - P_{ipred}\rvert\right)^2$
Root Mean Square Error (RMSE) [76]	$RMSE = \sqrt{\frac{1}{n}\sum_i \left(P_{iexp} - P_{ipred}\right)^2}$
Margin of deviation (MOD%) [81]	$MOD\% = \frac{P_{ipred} - P_{iexp}}{P_{iexp}} \times 100$

Conclusion

This study investigated the thermal conductivity of Al_2O_3/water nanofluid. RSM was effectively utilized in this study, yielding equations that accurately estimate the KR of the nanofluid. RSM provided different equations to calculate KR based on independent parameters such as SVF and T. The quadratic model has been demonstrated to be superior to the other models through statistical parameters and plots. R^2, adjusted R^2, predicted R^2 and Std. Dev parameters of the quadratic model were equal to 0.9785, 0.9606, 0.8776, and 0.0241, respectively, which signifies the model's accuracy. Also, the difference between adjusted R^2 and predicted R^2 is less than 0.083, indicating the high accuracy of the proposed model. The residual plot, the normal probability plot, the Box-Cox plot, and the predicted vs. actual plot also showed that the quadratic model has good accuracy and is capable of estimating the KR of the nanofluid. The experimental outcomes displayed that a rise in SVF and T caused an increase in KR. This trend was estimated using RSM methods with very high accuracy. Ultimately, the optimum combination for better KR was found at SVF = 1.764% and T = 45 ˚C.

Nomenclature

2FI	two-factor interaction
AAD	average absolute deviation
ANOVA	analysis of variance
C.D	correlation deviation
CV (%)	coefficient of Variation
D	Dimension
DF	degrees of Freedom
DLS	dynamic light scattering
EG	ethylene glycol
GNP	graphene nanoplatelets
GO	graphene oxide
H	Hour
HNF	hybrid nanofluid
KR	Thermal conductivity ratio (K_{nf}/K_{bf})
MOD	margin of deviation
MSE	mean square error
MWCNT	multi-walled carbon nanotubes
ND	Nanodiamond
R^2	coefficient of determination (-)
RSM	response surface methodology
SR	Shear rate
Std. Dev	standard deviation
SVF	solid volume fraction
T	Temperature (˚C)
TEM	Transmission electron microscopy
VIF	variance Inflation Factors
Vol	Volume
W	Water

Greek symbols

λ	lambda value

Subscripts

bf	base fluid
Exp	Experimental
Pred	Predicted

References

[1] Choi SU, Eastman JA. Enhancing thermal conductivity of fluids with nanoparticles. Argonne National Lab.(ANL), Argonne, IL (United States); 1995 Oct 1.

[2] Wang XJ, Zhu DS. Investigation of pH and SDBS on enhancement of thermal conductivity in nanofluids. Chemical Physics Letters. 2009 Feb 24;470(1-3):107-11. https://doi.org/10.1016/j.cplett.2009.01.035.

[3] Zhu D, Li X, Wang N, Wang X, Gao J, Li H. Dispersion behavior and thermal conductivity characteristics of Al2O3–H2O nanofluids. Current Applied Physics. 2009 Jan 1;9(1):131-9. https://doi.org/10.1016/j.cap.2007.12.008.

[4] Shahsavar A, Godini A, Sardari PT, Toghraie D, Salehipour H. Impact of variable fluid properties on forced convection of Fe 3 O 4/CNT/water hybrid nanofluid in a double-pipe mini-channel heat exchanger. Journal of Thermal Analysis and Calorimetry. 2019 Aug 15;137:1031-43. https://doi.org/10.1007/s10973-018-07997-6.

[5] Kumar N, Urkude N, Sonawane SS, Sonawane SH. Experimental study on pool boiling and Critical Heat Flux enhancement of metal oxides based nanofluid. International Communications in Heat and Mass Transfer. 2018 Aug 1;96:37-42. https://doi.org/10.1016/j.icheatmasstransfer.2018.05.018.

[6] Vijay J, Sonawane Shriram S. Investigations on rheological behaviour of paraffin based Fe3O4 nanofluids and its modelling. Res. J. Chem. Environ. 2015 Dec;19(12):22-9.

[7] Kumar N, Sonawane SS, Sonawane SH. Experimental study of thermal conductivity, heat transfer and friction factor of Al2O3 based nanofluid. International Communications in Heat and Mass Transfer. 2018 Jan 1;90:1-0. https://doi.org/10.1016/j.icheatmasstransfer.2017.10.001.

[8] Bhanvase BA, Barai DP, Sonawane SH, Kumar N, Sonawane SS. Intensified heat transfer rate with the use of nanofluids. In Handbook of nanomaterials for industrial applications 2018 Jan 1 (pp. 739-750). Elsevier. https://doi.org/10.1016/B978-0-12-813351-4.00042-0.

[9] Malika MM, Sonawane SS. Review on application of nanofluid/nano particle as water disinfectant. Journal of Indian Association for Environmental Management (JIAEM). 2019;39(1-4):21-4.

[10] Khan M, Mishra S, Ratna D, Sonawane S, Shimpi NG. Investigation of thermal and mechanical properties of styrene–butadiene rubber nanocomposites filled with SiO2–polystyrene core–shell nanoparticles. Journal of Composite Materials. 2020 Jun;54(14):1785-95.

[11] Yu W, Choi AS. The role of interfacial layers in the enhanced thermal conductivity of nanofluids: a renovated Maxwell model. Journal of nanoparticle research. 2003 Apr;5:167-71. https://doi.org/10.1023/A:1024438603801.

[12] Nadooshan AA. An experimental correlation approach for predicting thermal conductivity of water-EG based nanofluids of zinc oxide. Physica E: Low-dimensional Systems and Nanostructures. 2017 Mar 1;87:15-9. https://doi.org/10.1016/j.physe.2016.11.004.

[13] Esfe MH, Razi P, Hajmohammad MH, Rostamian SH, Sarsam WS, Arani AA, Dahari M. Optimization, modeling and accurate prediction of thermal conductivity and dynamic viscosity of stabilized ethylene glycol and water mixture Al2O3 nanofluids by NSGA-II using ANN. International Communications in Heat and Mass Transfer. 2017 Mar 1;82:154-60. https://doi.org/10.1016/j.icheatmasstransfer.2016.08.015.

[14] Esfe MH, Esfandeh S, Saedodin S, Rostamian H. Experimental evaluation, sensitivity analyzation and ANN modeling of thermal conductivity of ZnO-MWCNT/EG-water hybrid nanofluid for engineering applications. Applied Thermal Engineering. 2017 Oct 1;125:673-85. https://doi.org/10.1016/j.applthermaleng.2017.06.077.

[15] Esfe MH. Designing a neural network for predicting the heat transfer and pressure drop characteristics of Ag/water nanofluids in a heat exchanger. Applied Thermal Engineering. 2017 Nov 5;126:559-65. https://doi.org/10.1016/j.applthermaleng.2017.06.046.

[16] Heris SZ, Pour MB, Mahian O, Wongwises S. A comparative experimental study on the natural convection heat transfer of different metal oxide nanopowders suspended in turbine oil inside an inclined cavity. International Journal of Heat and Mass Transfer. 2014 Jun 1;73:231-8. https://doi.org/10.1016/j.ijheatmasstransfer.2014.01.071.

[17] Mahian O, Kianifar A, Heris SZ, Wongwises S. Natural convection of silica nanofluids in square and triangular enclosures: theoretical and experimental study. International Journal of Heat and Mass Transfer. 2016 Aug 1;99:792-804. https://doi.org/10.1016/j.ijheatmasstransfer.2016.03.045.

[18] Afrand M. Experimental study on thermal conductivity of ethylene glycol containing hybrid nano-additives and development of a new correlation. Applied Thermal Engineering. 2017 Jan 5;110:1111-9. https://doi.org/10.1016/j.applthermaleng.2016.09.024.

[19] Afrand M, Najafabadi KN, Akbari M. Effects of temperature and solid volume fraction on viscosity of SiO2-MWCNTs/SAE40 hybrid nanofluid as a coolant and lubricant in heat engines. Applied Thermal Engineering. 2016 Jun 5;102:45-54. https://doi.org/10.1016/j.applthermaleng.2016.04.002.

[20] Afrand M, Toghraie D, Sina N. Experimental study on thermal conductivity of water-based Fe3O4 nanofluid: development of a new correlation and modeled by artificial neural network. International Communications in Heat and Mass Transfer. 2016 Jul 1;75:262-9. https://doi.org/10.1016/j.icheatmasstransfer.2016.04.023.

[21] Esfe MH, Behbahani PM, Arani AA, Sarlak MR. Thermal conductivity enhancement of SiO2–MWCNT (85: 15%)–EG hybrid nanofluids. J Therm Anal Calorim. 2017 Apr;128(1):249-58. DOI 10.1007/s10973-016-5893-9.

[22] Esfe MH, Hajmohammad MH. Thermal conductivity and viscosity optimization of nanodiamond-Co3O4/EG (40: 60) aqueous nanofluid using NSGA-II coupled with RSM. Journal of Molecular Liquids. 2017 Jul 1;238:545-52. https://doi.org/10.1016/j.molliq.2017.04.056.

[23] Esfe MH, Ahangar MR, Rejvani M, Toghraie D, Hajmohammad MH. Designing an artificial neural network to predict dynamic viscosity of aqueous nanofluid of TiO2 using experimental data. International communications in heat and mass transfer. 2016 Jul 1;75:192-6. https://doi.org/10.1016/j.icheatmasstransfer.2016.04.002.

[24] Esfe MH, Hajmohammad MH, Razi P, Ahangar MR, Arani AA. The optimization of viscosity and thermal conductivity in hybrid nanofluids prepared with magnetic nanocomposite of nanodiamond cobalt-oxide (ND-Co3O4) using NSGA-II and RSM. International Communications in Heat and Mass Transfer. 2016 Dec 1;79:128-34. https://doi.org/10.1016/j.icheatmasstransfer.2016.09.015.

[25] Rostamian SH, Biglari M, Saedodin S, Esfe MH. An inspection of thermal conductivity of CuO-SWCNTs hybrid nanofluid versus temperature and concentration using experimental data, ANN modeling and new correlation. Journal of Molecular Liquids. 2017 Apr 1;231:364-9. https://doi.org/10.1016/j.molliq.2017.02.015.

[26] Zhang YY, Pei QX, Cheng Y, Zhang YW, Zhang X. Thermal conductivity of penta-graphene: the role of chemical functionalization. Computational Materials Science. 2017 Sep 1;137:195-200. https://doi.org/10.1016/j.commatsci.2017.05.042.

[27] Esfe MH, Yan WM, Afrand M, Sarraf M, Toghraie D, Dahari M. Estimation of thermal conductivity of Al2O3/water (40%)–ethylene glycol (60%) by artificial neural network and correlation using experimental data. International Communications in Heat and Mass Transfer. 2016 May 1;74:125-8. https://doi.org/10.1016/j.icheatmasstransfer.2016.02.002.

[28] Bashirnezhad K, Bazri S, Safaei MR, Goodarzi M, Dahari M, Mahian O, Dalkılıça AS, Wongwises S. Viscosity of nanofluids: a review of recent experimental studies. International Communications in Heat and Mass Transfer. 2016 Apr 1;73:114-23. https://doi.org/10.1016/j.icheatmasstransfer.2016.02.005.

[29] Hemmat Esfe M, Saedodin S, Mahian O, Wongwises S. Thermal conductivity of Al 2 O 3/water nanofluids: measurement, correlation, sensitivity analysis, and comparisons with literature reports. Journal of Thermal Analysis and Calorimetry. 2014 Aug;117:675-81. https://doi.org/10.1007/s10973-014-3771-x.

[30] Putra N, Roetzel W, Das SK. Natural convection of nano-fluids. Heat and mass transfer. 2003 Sep;39(8):775-84. https://doi.org/10.1007/s00231-002-0382-z.

[31] Zhang X, Gu H, Fujii M. Experimental study on the effective thermal conductivity and thermal diffusivity of nanofluids. International Journal of Thermophysics. 2006 Mar;27:569-80. https://doi.org/10.1007/s10765-006-0054-1.

[32] Masuda H, Ebata A, Teramae K. Alteration of thermal conductivity and viscosity of liquid by dispersing ultra-fine particles. Dispersion of Al2O3, SiO2 and TiO2 ultra-fine particles.

[33] Eastman JA, Choi SU, Li S, Yu W, Thompson LJ. Anomalously increased effective thermal conductivities of ethylene glycol-based nanofluids containing copper nanoparticles. Applied physics letters. 2001 Feb 5;78(6):718-20. https://sid.ir/paper/596250/en.

[34] Murshed SM, Leong KC, Yang C. Enhanced thermal conductivity of TiO2—water based nanofluids. International Journal of thermal sciences. 2005 Apr 1;44(4):367-73. https://doi.org/10.1016/j.ijthermalsci.2004.12.005.

[35] Mintsa HA, Roy G, Nguyen CT, Doucet D. New temperature dependent thermal conductivity data for water-based nanofluids. International journal of thermal sciences. 2009 Feb 1;48(2):363-71. https://doi.org/10.1016/j.ijthermalsci.2008.03.009.

[36] Abdel-Samad, S.M., et al., Experimental investigation of TiO2-water nanofluids thermal conductivity synthesized by Sol-gel technique. Current Nanoscience, 2017. **13**(6): p. 586-594. http://dx.doi.org/10.2174/1573413713666170619124221.

[37] Eshgarf H, Nadooshan AA, Raisi A, Afrand M. Experimental examination of the properties of Fe3O4/water nanofluid, and an estimation of a correlation using an artificial neural network. Journal of Molecular Liquids. 2023 Mar 15;374:121150. http://dx.doi.org/10.1016/j.molliq.2022.121150.

[38] Jahan A, Edwards KL, Bahraminasab M. Multi-criteria decision analysis for supporting the selection of engineering materials in product design. Butterworth-Heinemann; 2016 Feb 17.

[39] Malika M, Sonawane SS. Application of RSM and ANN for the prediction and optimization of thermal conductivity ratio of water based Fe2O3 coated SiC hybrid nanofluid. International Communications in Heat and Mass Transfer. 2021 Jul 1;126:105354. https://doi.org/10.1016/j.icheatmasstransfer.2021.105354.

[40] Esfe MH, Firouzi M, Afrand M. Experimental and theoretical investigation of thermal conductivity of ethylene glycol containing functionalized single walled carbon nanotubes. Physica E: Low-dimensional Systems and Nanostructures. 2018 Jan 1;95:71-7. https://doi.org/10.1016/j.physe.2017.08.017.

[41] Peng Y, Khaled U, Al-Rashed AA, Meer R, Goodarzi M, Sarafraz MM. Potential application of Response Surface Methodology (RSM) for the prediction and optimization of thermal conductivity of aqueous CuO (II) nanofluid: A statistical

approach and experimental validation. Physica A: Statistical Mechanics and its Applications. 2020 Sep 15;554:124353. https://doi.org/10.1016/j.physa.2020.124353.
[42] Esfe, M.H., et al., The effect of different parameters on ability of the proposed correlations for the rheological behavior of SiO2-MWCNT (90: 10)/SAE40 oil-based hybrid nano-lubricant and presenting five new correlations. ISA transactions, 2022. **128**: p. 488-497. https://doi.org/10.1016/j.isatra.2021.10.012.
[43] Khetib Y, Abo-Dief HM, Alanazi AK, Rawa M, Sajadi SM, Sharifpur M. Competition of ANN and RSM techniques in predicting the behavior of the CuO-liquid paraffin. Chemical Engineering Communications. 2023 Jun 3;210(6):880-92. https://doi.org/10.1080/00986445.2021.1980398.
[44] Esfe MH, Firouzi M, Rostamian H, Afrand M. Prediction and optimization of thermophysical properties of stabilized Al2O3/antifreeze nanofluids using response surface methodology. Journal of Molecular Liquids. 2018 Jul 1;261:14-20. https://doi.org/10.1016/j.molliq.2018.03.063.
[45] Khetib Y, Alahmadi A, Alzaed A, Sajadi SM, Vaziri R, Sharifpur M. Using neural network and RSM to evaluate improvement in thermal conductivity of nanodiamond-iron oxide/antifreeze. Chemical Engineering Communications. 2023 Apr 3;210(4):596-606. https://doi.org/10.1080/00986445.2021.1974417.
[46] Khetib Y, Sedraoui K, Gari A. Improving thermal conductivity of a ferrofluid-based nanofluid using Fe3O4-challenging of RSM and ANN methodologies. Chemical Engineering Communications. 2022 May 23;209(8):1070-81. https://doi.org/10.1080/00986445.2021.1943369.
[47] Shahsavar A, Sepehrnia M, Maleki H, Darabi R. Thermal conductivity of hydraulic oil-GO/Fe3O4/TiO2 ternary hybrid nanofluid: experimental study, RSM analysis, and development of optimized GPR model. Journal of Molecular Liquids. 2023 Sep 1;385:122338. https://doi.org/10.1016/j.molliq.2023.122338.
[48] Borode A, Olubambi P. Modelling the effects of mixing ratio and temperature on the thermal conductivity of GNP-Alumina hybrid nanofluids: A comparison of ANN, RSM, and linear regression methods. Heliyon. 2023 Aug 1;9(8). https://doi.org/10.1016/j.heliyon.2023.e19228.
[49] Esfe MH, Toghraie D, Esfandeh S, Alidoust S. Measurement of thermal conductivity of triple hybrid water based nanofluid containing MWCNT (10%)-Al2O3 (60%)-ZnO (30%) nanoparticles. Colloids and Surfaces A: Physicochemical and Engineering Aspects. 2022 Aug 20;647:129083. https://doi.org/10.1016/j.colsurfa.2022.129083.
[50] Esfe MH, Alidoust S, Tamrabad SN, Toghraie D, Hatami H. Thermal conductivity of MWCNT-TiO2/Water-EG hybrid nanofluids: Calculating the price performance factor (PPF) using statistical and experimental methods (RSM). Case Studies in Thermal Engineering. 2023 Aug 1;48:103094. https://doi.org/10.1016/j.csite.2023.103094.
[51] Mukherjee S, Mishra PC, Chaudhuri P. Stability of heat transfer nanofluids–a review. ChemBioEng Reviews. 2018 Oct;5(5):312-33. https://doi.org/10.1002/cben.201800008.
[52] Raei B, Shahraki F, Jamialahmadi M, Peyghambarzadeh SM. Experimental study on the heat transfer and flow properties of γ-Al 2 O 3/water nanofluid in a double-tube heat exchanger. Journal of Thermal Analysis and Calorimetry. 2017 Mar;127:2561-75. https://doi.org/10.1007/s10973-016-5868-x.
[53] Raei, B., et al., Experimental investigation on the heat transfer performance and pressure drop characteristics of γ-Al2O3/water nanofluid in a double tube counter flow heat exchanger. Challenges in Nano and Micro Scale Science and Technology, 2016. **5**(1): p. 64-75. https://doi.org/10.7508/tpnms.2017.01.007.
[54] Raei B. Statistical analysis of nanofluid heat transfer in a heat exchanger using Taguchi method. Journal of heat and mass transfer research. 2021 Jun 1;8(1):29-38. https://doi.org/10.22075/jhmtr.2020.20678.1287.

[55] Raei B, Peyghambarzadeh SM, Asl RS. Experimental investigation on heat transfer and flow resistance of drag-reducing alumina nanofluid in a fin-and-tube heat exchanger. Applied Thermal Engineering. 2018 Nov 5;144:926-36. https://doi.org/10.1016/j.applthermaleng.2018.09.006.

[56] Raei, B. and S.M. Peyghambarzadeh, Measurement of Local Convective Heat Transfer Coefficient of Alumina-Water Nanofluids in a Double Tube Heat Exchanger. Journal of Chemical and Petroleum engineering, 2019. **53**(1): p. 25-36. https://doi.org/10.22059/jchpe.2019.265521.1247.

[57] Mukherjee S, Panda SR, Mishra PC, Chaudhuri P. Enhancing thermophysical characteristics and heat transfer potential of TiO 2/water nanofluid. International Journal of Thermophysics. 2020 Dec;41:1-33. https://doi.org/10.1007/s10765-020-02745-1.

[58] Ali N, Teixeira JA, Addali A. A review on nanofluids: fabrication, stability, and thermophysical properties. Journal of Nanomaterials. 2018;2018(1):6978130. https://doi.org/10.1155/2018/6978130.

[59] Cabaleiro D, Colla L, Barison S, Lugo L, Fedele L, Bobbo SJ. Heat transfer capability of (ethylene glycol+ water)-based nanofluids containing graphene nanoplatelets: Design and thermophysical profile. Nanoscale research letters. 2017 Dec;12:1-1. https://doi.org/10.1186/s11671-016-1806-x.

[60] Fedele L, Colla L, Bobbo S, Barison S, Agresti F. Experimental stability analysis of different water-based nanofluids. Nanoscale research letters. 2011 Dec;6:1-8. https://doi.org/10.1186/1556-276X-6-300.

[61] Teng TP, Hung YH, Teng TC, Mo HE, Hsu HG. The effect of alumina/water nanofluid particle size on thermal conductivity. Applied Thermal Engineering. 2010 Oct 1;30(14-15):2213-8. https://doi.org/10.1016/j.applthermaleng.2010.05.036.

[62] Sodeifian GH, Azizi J, Ghoreishi SM. Response surface optimization of Smyrnium cordifolium Boiss (SCB) oil extraction via supercritical carbon dioxide. The Journal of Supercritical Fluids. 2014 Nov 1;95:1-7. https://doi.org/10.1016/j.supflu.2014.07.023.

[63] Sodeifian G, Saadati Ardestani N, Sajadian SA. Extraction of seed oil from Diospyros lotus optimized using response surface methodology. Journal of forestry research. 2019 Apr 15;30:709-19. https://doi.org/10.1007/s11676-018-0631-8.

[64] Sodeifian G, Ardestani NS, Sajadian SA, Moghadamian K. Properties of Portulaca oleracea seed oil via supercritical fluid extraction: Experimental and optimization. The Journal of Supercritical Fluids. 2018 May 1;135:34-44. https://doi.org/10.1016/j.supflu.2017.12.026.

[65] Sodeifian G, Sajadian SA, Honarvar B. Mathematical modelling for extraction of oil from Dracocephalum kotschyi seeds in supercritical carbon dioxide. Natural product research. 2018 Apr 3;32(7):795-803. https://doi.org/10.1080/14786419.2017.1361954.

[66] Sodeifian G, Sajadian SA, Ardestani NS. Experimental optimization and mathematical modeling of the supercritical fluid extraction of essential oil from Eryngium billardieri: Application of simulated annealing (SA) algorithm. The journal of supercritical fluids. 2017 Sep 1;127:146-57. https://doi.org/10.1016/j.supflu.2017.04.007.

[67] Ameri A, Sodeifian G, Sajadian SA. Lansoprazole loading of polymers by supercritical carbon dioxide impregnation: Impacts of process parameters. The Journal of Supercritical Fluids. 2020 Oct 1;164:104892. https://doi.org/10.1016/j.supflu.2020.104892.

[68] Fathi M, Sodeifian G, Sajadian SA. Experimental study of ketoconazole impregnation into polyvinyl pyrrolidone and hydroxyl propyl methyl cellulose using supercritical carbon dioxide: Process optimization. The Journal of Supercritical Fluids. 2022 Sep 1;188:105674. https://doi.org/10.1016/j.supflu.2022.105674.

[69] Ardestani, N.S., G. Sodeifian, and S.A. Sajadian, Preparation of phthalocyanine green nano pigment using supercritical CO2 gas antisolvent (GAS): experimental and modeling. Heliyon, 2020. 6(9). https://doi.org/10.1016/j.heliyon.2020.e04947.

[70] Sodeifian G, Sajadian SA, Derakhsheshpour R. CO2 utilization as a supercritical solvent and supercritical antisolvent in production of sertraline hydrochloride

nanoparticles. Journal of CO2 Utilization. 2022 Jan 1;55:101799. https://doi.org/10.1016/j.jcou.2021.101799.

[71] Hazaveie SM, Sodeifian G, Ardestani NS. Micro and nanosizing of Tamsulosin drug via supercritical CO2 antisolvent (SAS) process. Journal of CO2 Utilization. 2024 Jun 1;84:102847. https://doi.org/10.1016/j.jcou.2024.102847.

[72] Lau HL, Wong FW, Abd Rahman RN, Mohamed MS, Ariff AB, Hii SL. Optimization of fermentation medium components by response surface methodology (RSM) and artificial neural network hybrid with genetic algorithm (ANN-GA) for lipase production by Burkholderia cenocepacia ST8 using used automotive engine oil as substrate. Biocatalysis and Agricultural Biotechnology. 2023 Jul 1;50:102696. https://doi.org/10.1016/j.bcab.2023.102696.

[73] Hussain S, Khan H, Gul S, Steter JR, Motheo AJ. Modeling of photolytic degradation of sulfamethoxazole using boosted regression tree (BRT), artificial neural network (ANN) and response surface methodology (RSM); energy consumption and intermediates study. Chemosphere. 2021 Aug 1;276:130151. https://doi.org/10.1016/j.chemosphere.2021.130151.

[74] Borode AO, Ahmed NA, Olubambi PA, Sharifpur M, Meyer JP. Effect of various surfactants on the viscosity, thermal and electrical conductivity of graphene nanoplatelets nanofluid. International Journal of Thermophysics. 2021 Nov;42(11):158. https://doi.org/10.1007/s10765-021-02914-w.

[75] Amiri A, Shanbedi M, Dashti H. Thermophysical and rheological properties of water-based graphene quantum dots nanofluids. Journal of the Taiwan Institute of Chemical Engineers. 2017 Jul 1;76:132-40. https://doi.org/10.1016/j.jtice.2017.04.005.

[76] Rostamian H, Lotfollahi MN. A novel statistical approach for prediction of thermal conductivity of CO2 by Response Surface Methodology. Physica A: Statistical Mechanics and its Applications. 2019 Aug 1;527:121175. https://doi.org/10.1016/j.physa.2019.121175.

[77] Wasp EJ, Kenny JP, Gandhi RL. Solid--liquid flow: slurry pipeline transportation. [Pumps, valves, mechanical equipment, economics]. Ser. Bulk Mater. Handl.;(United States). 1977 Jan 1;1(4).

[78] Williams AJ. Expendable benthic lander (XBL). In2008 IEEE/OES US/EU-Baltic International Symposium 2008 May 27 (pp. 1-8). IEEE.

[79] Ho CJ, Liu WK, Chang YS, Lin CC. Natural convection heat transfer of alumina-water nanofluid in vertical square enclosures: An experimental study. International Journal of Thermal Sciences. 2010 Aug 1;49(8):1345-53. https://doi.org/10.1016/j.ijthermalsci.2010.02.013.

[80] Rostamian H, Lotfollahi MN. A new simple equation of state for calculating solubility of solids in supercritical carbon dioxide. Periodica Polytechnica Chemical Engineering. 2015 Feb 18;59(3):174-85. https://doi.org/10.3311/PPch.7714.

[81] Zhao TH, Castillo O, Jahanshahi H, Yusuf A, Alassafi MO, Alsaadi FE, Chu YM. A fuzzy-based strategy to suppress the novel coronavirus (2019-NCOV) massive outbreak. Applied and Computational Mathematics. 2021 Jan 1;20(1):160-76.

How to cite: Raei B. Modeling and Optimization of Thermal Conductivity of Stabilized γ-Al_2O_3 /Water Nanofluid Using Response Surface Methodology (RSM). Journal of Chemical and Petroleum Engineering 2025; 59(1): 1-22.